EUROPEAN ORGANIZATION FOR NUCLEAR RESEARCH

CERN-PPE/96-73
May 30, 1996

Measurement of the B_d^0 Meson Oscillation Frequency

L3 Collaboration

Abstract

Time-dependent B_d^0-$\bar{B}_d^0$ mixing is studied using 1.5 million hadronic Z decays collected by L3. Semileptonic B decays are selected by requiring at least one reconstructed lepton in both thrust hemispheres. Charge correlations between the tagged leptons are studied as a function of proper time. The proper time of the b-hadron decay is measured by reconstructing the production and decay vertices using a silicon microvertex detector. The measured B_d^0 meson oscillation frequency corresponds to a mass difference Δm_d between the two B_d^0 mass eigenstates of

$$\Delta m_d = \left(0.496^{+0.055}_{-0.051}\ (\mathrm{stat}) \pm 0.043\ (\mathrm{syst})\right)\ \mathrm{ps}^{-1}.$$

(Submitted to *Physics Letters B)*

Introduction

As in the case of K-mesons, oscillations between particle-antiparticle states are expected in neutral B-mesons. In the Standard Model, the mechanism causing mixing is a second-order weak interaction through box diagrams. The flavour eigenstates $\mathrm{B_d^0}$ $(\bar{\mathrm{b}}\mathrm{d})$ and $\bar{\mathrm{B}}_\mathrm{d}^0(\mathrm{b}\bar{\mathrm{d}})$ are linear combinations of the mass eigenstates $\mathrm{B_1}$ and $\mathrm{B_2}$. Neglecting the decay width difference between $\mathrm{B_1}$ and $\mathrm{B_2}$ and the effects of CP violation, both expected to be small, the probability P to find a $\mathrm{B_d^0}$ decaying at proper time t, provided it was produced as $\bar{\mathrm{B}}_\mathrm{d}^0$ at $t = 0$, is given by

$$P(\bar{\mathrm{B}}_\mathrm{d}^0 \rightarrow \mathrm{B_d^0}) = \frac{1}{\tau} e^{-\frac{t}{\tau}} \left(\frac{1 - \cos \Delta m_d \, t}{2} \right)$$

where τ is the lifetime of the B meson. A measurement of the oscillation frequency thus gives a direct measurement of the mass difference Δm_d between the two mass eigenstates.

The phenomenon of $\mathrm{B^0}$-$\bar{\mathrm{B}}^0$ mixing is well established by experiment. Time-integrated probabilities for mixing in the $\mathrm{B^0}$-$\bar{\mathrm{B}}^0$ system were first measured by the UA1 Collaboration [1] for a mixture of $\mathrm{B_d^0}$ and $\mathrm{B_s^0}$ mesons. Mixing of $\mathrm{B_d^0}$-$\bar{\mathrm{B}}_\mathrm{d}^0$ alone was measured at the Υ(4S) by the ARGUS and CLEO [2] experiments. Precise measurements of $\mathrm{B^0}$-$\bar{\mathrm{B}}^0$ mixing have been obtained at LEP [3] for a mixture of $\mathrm{B_d^0}$ and $\mathrm{B_s^0}$ mesons. The time dependence of mixing for $\mathrm{B_d^0}$ mesons has been recently studied at LEP using various techniques [4–6].

Here we present a measurement of the $\mathrm{B_d^0}$ oscillation frequency with the L3 detector. For this study we use dileptons in opposite hemispheres to tag the flavour of the b-hadrons in $\mathrm{Z} \rightarrow \mathrm{b}\bar{\mathrm{b}}$ decays. The signature for mixing is the presence of same-sign lepton pairs. Proper time is measured by reconstructing primary and secondary vertices. The dilepton sample corresponds to about 1.5 million hadronic Z decays recorded in 1994.

In the following sections we describe the L3 detector, the event and lepton selections, the proper time reconstruction, the fitting procedure and the results of the measurement of $\mathrm{B_d^0}$-$\bar{\mathrm{B}}_\mathrm{d}^0$ oscillations.

The L3 Detector

The L3 detector is described in detail in reference 7. It consists of a central tracking chamber, a high-resolution electromagnetic calorimeter composed of bismuth germanium oxide (BGO) crystals, a ring of plastic scintillation counters, a uranium and brass hadron calorimeter with proportional wire chamber readout and a high resolution muon chamber system. These detectors are installed in a 12 m diameter magnet which provides a uniform field of 0.5 T along the beam direction.

The muon spectrometer, located outside the hadron calorimeter, consists of three layers of drift chambers which measure 56 points on the muon trajectory in the bending plane (r-ϕ) and 8 points in the non-bending direction (z).

The material preceding the barrel part of the electromagnetic calorimeter amounts to less than 10% of a radiation length. In this region the energy resolution of the BGO calorimeter is better than 2% and the angular resolution of electromagnetic clusters is better than 0.5° for energies above 1 GeV.

The central tracking chamber is a time expansion chamber (TEC) which consists of two cylindrical layers of 12 and 24 sectors, with a total of 62 wires measuring r-ϕ coordinates. The single wire resolution ranges from 35 μm to 100 μm depending on the drift distance. A chamber mounted just outside the TEC provides z coordinate measurements.

A Silicon Microvertex Detector (SMD) was installed inside the L3 detector during 1993. It consists of two cylindrical layers of double-sided silicon microstrip detectors, placed at 6 cm and 8 cm from the beam axis, respectively, covering $\approx 90\%$ of the solid angle. Each layer consists of 12 basic modules, constructed out of four silicon sensors 70 mm long, 40 mm wide and 300 μm thick, with a readout pitch of 50 μm on the junction (r-ϕ) side and 150/200 μm on the ohmic (z) side. The intrinsic resolution of the SMD is 7 μm on the junction side and 15 μm on the ohmic side [8].

Tracks are first reconstructed in the TEC. They are then extrapolated to the SMD layers and refitted using the matched SMD hits.

Event Selection

Hadronic events are selected by the following cuts:

- total calorimetric energy $E_{cal} > 38$ GeV;
- longitudinal energy imbalance $|E_{||}|/E_{vis} < 0.5$;
- transverse energy imbalance $|E_{\perp}|/E_{vis} < 0.5$.

E_{vis} is the sum of the calorimetric energy and the energy of any muon observed in the muon spectrometer; $E_{||}$ and $E_{\perp}$ are, respectively, the energy flow parallel and transverse to the beam direction.

- energy of the most energetic jet [7] > 10 GeV;
- at least 15 calorimetric clusters;
- at least 5 tracks which include a hit from the inner r-ϕ layer of the SMD.

Lepton Identification

Events are classified as dilepton events if there is at least one lepton candidate in each event hemisphere defined by the thrust axis. If there are several lepton candidates in the same hemisphere, only the one with the highest momentum is considered for charge assignment and secondary vertex reconstruction. The lepton is associated to a jet.

Selection of muon candidates

Muon candidates are selected by the following criteria:

- tracks found in the barrel muon system ($|\cos\theta| < 0.82$) must be reconstructed in at least two of the three r-ϕ chamber layers and one of the two z chamber layers.
- The measured muon momentum must be greater than 4 GeV and the measured muon transverse momentum p_t with respect to the associated jet must be greater than 1 GeV. We exclude the muon from the jet for the calculation of p_t.

- The reconstructed muon track must come from the collision region: the transverse (r-ϕ plane) distance to the average interaction point must be less than three times its error and at most 300 mm. The longitudinal (z) distance must be less than four times its error and at most 400 mm. On average the errors on transverse and longitudinal distances are 40 mm and 50 mm, respectively.

- a match is required between the track reconstructed in the muon detector and a track from the inner tracker system.

Selection of electron candidates

Electron candidates are selected by the following criteria:

- The energy of a cluster in the barrel of the BGO calorimeter (selected with a polar angle $|\cos\theta| < 0.69$) must be greater than 3 GeV and the measured electron transverse momentum with respect to the associated jet must be greater than 1 GeV. The electron candidate is excluded from the jet in the calculation of its transverse momentum.

- The lateral shower shape of the BGO cluster must be consistent with that of an electromagnetic shower: $E_{9/25} > 0.9$, where $E_{9/25}$ is the ratio of the energy deposited in 9 crystals around the shower center to the energy of 25 crystals. The number of crystals associated with the BGO cluster must be more than 9.

- To suppress hadrons further, the energy in the hadron calorimeter inside a cone around the electron candidate is required to be less than 3 GeV. The cone is centered on the BGO cluster and has a half opening angle of 7°.

- The difference between the azimuthal angles estimated from the shower center and from the track impact point at the BGO calorimeter must be smaller than 5 mrad. The BGO cluster must be matched to a track satisfying the matching in energy $E/p < 2$, where E is the energy of the cluster measured in the BGO and p is the momentum of the matching track as measured in the central tracker. For the projection on the r-ϕ plane, $E_{\perp}$ and $p_{\perp}$, we require $|1/E_{\perp} - 1/p_{\perp}| < 0.07 \ \ \mathrm{GeV}^{-1}$.

The numbers of selected inclusive lepton and dilepton events are given in Table 1. The JETSET 7.3 Monte Carlo program [9] was used to generate hadronic Z decays. The detector simulation was performed by a GEANT-based description of the L3 detector [10]. The fragmentation of b quarks was modeled using the fragmentation function of Peterson et al. [11] with an average energy of b-hadrons $\langle x_E \rangle = 0.70\ E_{beam}$. More details about the generation of weak decays of c- and b-hadrons are given in Reference 12. Parameters of the generation relevant for the present analysis are given in Table 2.

Momentum and transverse momentum spectra of muon and electron candidates in dilepton events are shown in Figure 1 for data and Monte Carlo. The Monte Carlo spectra are normalized to the same luminosity as the data.

Proper Time Reconstruction

To estimate the decay length of a b-hadron candidate one needs to determine the primary and secondary vertex positions. Vertex finding is performed in the r-ϕ plane. The direction of the

Event type	Number of events	b-purity (%) (no vertex finding)
lepton + hadrons	45876	77
e + hadrons	22231	73
μ + hadrons	23645	80
2 *leptons* + hadrons	1600	98
ee + hadrons	334	97
$e\mu$ + hadrons	779	99
$\mu\mu$ + hadrons	487	98

Table 1: The number of inclusive lepton and dilepton events used in this analysis.

Parameter	Value
b lifetime (ps)	1.55
$\mathrm{Br}(\mathrm{b} \to \mathrm{l})$	0.1068
$\mathrm{Br}(\mathrm{b} \to \mathrm{c} \to \mathrm{l})$	0.08
$\mathrm{Br}(\mathrm{b} \to \bar{\mathrm{c}} \to \mathrm{l})$	0.014
χ_s	0.48

Table 2: The parameters used in the simulation. χ_s is the time-integrated mixing probability for $\mathrm{B_s^0}$ mesons.

jet containing the lepton is then used to obtain a three-dimensional decay length. A subsample of good tracks is first selected requiring for each track at least 26 hits with a span of at least 36 wires[1)], a momentum in the r-ϕ plane be greater than 0.2 GeV and a distance of closest approach (DCA) to the average position of the $\mathrm{e^+e^-}$ collision point in the r-ϕ plane be less than 10 mm.

These requirements exclude poorly reconstructed tracks, tracks with large curvature and tracks from decays of long-lived particles. The requirements on the number of hits and their span ensures an accurate extrapolation of the track to the sensitive volume of the SMD and to the interaction region. On average 17 tracks survive these cuts in dilepton hadronic events.

The proper time of the b-hadron decay is reconstructed as follows:

- Primary vertex

The primary vertex in the r-ϕ plane is reconstructed event by event in an iterative procedure starting from the known average position of the collision point[2)]. Only tracks with SMD inner r-

[1)]The span is the distance between the first and the last hit in units of the wire spacing.
[2)]This point is determined on a fill by fill basis by fitting all tracks in Z decays to a common vertex.

ϕ layer information are considered. Lepton candidates and tracks with a DCA to the candidate vertex greater than two times its estimated error are excluded. The error estimate includes the error on the vertex position itself, the track measurement error and a contribution from multiple scattering. The average position of the collision point and its effective spread are used to constrain the primary vertex fit. The iteration procedure stops if the difference between two iterations is less than 3 μm or after 10 iterations. The procedure usually converges after a few iterations. We require at least three tracks for the primary vertex reconstruction. The primary vertex resolution depends on the number of tracks selected for its reconstruction, on the event thrust value and direction and on the number of secondary vertex tracks erroneously included as primary vertex tracks. The resolution for the primary vertex reconstruction in the horizontal projection (x) for $b\bar{b}$ events is about 80 μm. As the vertical position (y) of the average collision point is known with better precision (about 20 μm), we take this position as y coordinate of the primary vertex. The reconstruction efficiency of the primary vertex is 95%.

- Secondary vertex

A secondary vertex reconstruction is attempted for each jet containing a lepton using tracks not included in the primary vertex determination. The lepton is always included as a secondary vertex track. With this approach we combine into one vertex tracks from the decay of the b-hadron as well as tracks from subsequent decays. On average 2.9 tracks are used in the calculation of the B decay vertex position. The average efficiency to reconstruct a secondary vertex is 70%. The efficiency drops significantly for small decay lengths, where the secondary vertex becomes indistinguishable from the primary one.

- Decay length

The decay length is the distance between primary and secondary vertex reconstructed in the r-ϕ plane and converted to a three-dimensional decay length by $l = l_{xy}/\sin\theta_{jet}$ where θ_{jet} is the polar angle of the jet containing the lepton. In our analysis, dilepton events with at least one measured decay length are selected. This gives a sample of 1340 events with 1862 decay lengths measured. Additional quality cuts for the decay length measurement are then applied. We require that the error estimate for the decay length reconstruction is less than 1 mm. Negative values of the decay length, due to resolution, should be no further than three standard deviations away from zero. With these requirements, 1107 dilepton events with 1429 secondary vertices remain. Figure 2 shows the distribution of the difference between the reconstructed decay length and the true decay length for Monte Carlo events. As expected, this distribution is biased towards positive values since the secondary vertex reconstruction includes tracks coming from the B decay vertex and also from the subsequent D decay vertex. The resolution is constant in the whole range except at small decay lengths where the track assignment to each vertex is not as reliable.

- Proper time measurement

The proper time t is related to the decay length in the laboratory system by $t = lm_B/p_B$ where m_B and p_B are the mass and momentum of the b-hadron. m_B is taken to be 5.3 GeV. For the momentum of the b-hadron we have used a constant fraction of the beam energy. Various fractions of the beam energy were tried and the value $p_B = 0.85\ E_{beam}$ was found to optimize the proper time resolution. The average resolutions of a three Gaussian fit are 0.29, 0.91 and

2.8 ps (the expected period of B^0_d oscillation corresponds to about 14 ps) and the corresponding fractions are 0.40, 0.47 and 0.13. The proper time resolution is a function of proper time itself and the dependence is parametrized in 17 subintervals of the true proper time range with three Gaussians per interval. As an example we show the proper time distribution obtained from Monte Carlo for four slices in Figure 3.

Fitting Procedure

The samples containing like-sign and unlike-sign lepton pairs are analysed using an unbinned maximum-likelihood method. A likelihood is assigned to each event proportional to the probability density to find such an event at the measured decay time or decay times if both have been measured.

The likelihood for a single event with both proper times t_1 and t_2 measured is given by

$$\begin{aligned} \mathcal{L}_{like}(t_1,t_2) &= P_r(t_1)P_w(t_2) + P_w(t_1)P_r(t_2) \\ \mathcal{L}_{unlike}(t_1,t_2) &= P_r(t_1)P_r(t_2) + P_w(t_1)P_w(t_2) \end{aligned}$$

for like-sign and unlike-sign events, respectively. $P_r(t)$ is the probability to find, at proper time t, a lepton with the "right" sign of charge, i.e. with the expected sign for a b-quark decay without mixing. $P_w(t)$ is the probability of finding a "wrong" sign opposite to the one expected at proper time t. The presence of "wrong" signs can be due to mixing, leptons from cascade decays, fake leptons or the contribution of light-quark events passing the event and lepton selections. Decomposing the probability $P_w(t)$ into these contributions one gets

$$\begin{aligned} P_w(t) \quad &= F_{bl}[(1-w_{bl})Q_{bl,mix}(t) + w_{bl}((1-f_d-f_s)Q_{bl,dec}(t) + Q_{bl,unm}(t))] \\ &+F_{bcl}[(1-w_{bcl})Q_{bcl,mix}(t) + w_{bcl}((1-f_d-f_s)Q_{bcl,dec}(t) + Q_{bcl,unm}(t))] \\ &+F_{bfk}[(1-w_{bfk})Q_{bfk,mix}(t) + w_{bfk}((1-f_d-f_s)Q_{bfk,dec}(t) + Q_{bfk,unm}(t))] \\ &+F_{cc}w_{cc}Q_{cc}(t) \\ &+F_{uds}w_{uds}Q_{uds}(t) \end{aligned}$$

The probability function $P_r(t)$ is obtained from $P_w(t)$ by exchanging w and $(1-w)$.

Here f_d and f_s are the fractions of B^0_d and B^0_s mesons in the sample; F_{bl}, F_{bcl}, F_{bfk}, F_{cc}, F_{uds} are the fractions of the various types of events: leptons coming from semileptonic decays of b-hadrons, cascade decays ($b \to c \to l$, $b \to \bar{c} \to l$, $b \to J \to l^+l^-$), fake leptons in $b\bar{b}$ events, lepton candidates from $c\bar{c}$ events and $u\bar{u}$, $d\bar{d}$ and $s\bar{s}$ events, respectively.

The w factors (w_{bl}, w_{bcl}, w_{bfk}, w_{cc} and w_{uds}) give the probabilities to find a lepton sign opposite to the one expected if the event resulted from an unmixed B decay. For direct $b \to l$ decays, this probability is the fraction of wrong lepton signs due to charge confusion and is very small. For cascade decays it is close to one. For fake leptons, there is a non-vanishing probability to have the same charge as for true leptons from unmixed B decay. These three b-related w factors are determined from Monte Carlo $b\bar{b}$ events. The w factors for $c\bar{c}$ -events are those describing the probability to get like-sign pairs in Monte Carlo $c\bar{c}$ events. For uds-events the w factors are fixed to be 0.5.

For $b\bar{b}$ events, in the probabilities $Q_{i,j}(t)$ the index i (=bl, bcl, bfk) labels the various types of events, and the index j (=mix, unm, dec) labels the cases of mixed and unmixed decays of neutral B-mesons, decays of charged B-mesons and b-baryons, respectively. These probabilities are convolutions of the probability density functions for the corresponding decays with a resolution function $R(t,t')$ which describes the probability of finding an event at the measured time t when it occurred at time t'. For instance,

$$Q_{i,mix}(t) = f_d \int_0^\infty \frac{1}{\tau} e^{-\frac{t'}{\tau}} \left(\frac{1-\cos \Delta m_d t'}{2} \right) R(t,t')dt'$$

$$+ f_s \int_0^\infty \frac{1}{\tau} e^{-\frac{t'}{\tau}} \left(\frac{1-\cos \Delta m_s t'}{2} \right) R(t,t')dt'$$

where Δm_d and Δm_s are the oscillation frequencies of B_d^0 and B_s^0 mesons. $Q_{i,unm}(t)$ has the same form except for an opposite sign in front of $\cos \Delta m\, t'$. The normalized decay probability for decays without mixing is given by

$$Q_{i,dec}(t) = \int_0^\infty \frac{1}{\tau} e^{-\frac{t'}{\tau}} R(t,t')dt'.$$

For non-$b\bar{b}$ events, the probability density functions $Q_{cc}(t)$ and $Q_{uds}(t)$ are defined by a parametrization of the corresponding Monte Carlo distributions for reconstructed decay times.

All fractions F and factors w for dilepton events are listed in Table 3 where by convention the first lepton is the most energetic one.

source	first lepton		second lepton	
	F	w	F	w
$b \to l$	0.882	0.004	0.836	0.004
cascade	0.067	0.89	0.115	0.78
fakes	0.043	0.31	0.041	0.31
$c\bar{c}$-events	0.006	0.0	0.006	0.38
$u\bar{u}, d\bar{d}, s\bar{s}$-events	0.002	0.50	0.002	0.50

Table 3: Fractions F and factors w for dilepton events from Monte Carlo. The first lepton is the most energetic one.

In the cases when only one lepton has a time measurement the probability function of the lepton with no time measurement is:

$$\begin{aligned} P_w \quad &= F_{bl}[(1-w_{bl})\overline{\chi} + w_{bl}(1-\overline{\chi})] \\ &+F_{bcl}[(1-w_{bcl})\overline{\chi} + w_{bcl}(1-\overline{\chi})] \\ &+F_{bfk}[(1-w_{bfk})\overline{\chi} + w_{bfk}(1-\overline{\chi})] \\ &+F_{cc}w_{cc} + F_{uds}w_{uds}, \end{aligned}$$

where $\overline{\chi} = (f_d\chi_d + f_s\chi_s)$, $\chi_d(\Delta m_d)$ and $\chi_s(\Delta m_s)$ are the time-integrated mixing probabilities including all reconstruction efficiencies for B_d^0 and B_s^0 mesons.

The total likelihood $\mathcal{L}$ for the full event sample is calculated as the product of likelihood functions $\mathcal{L}_{like}$ or $\mathcal{L}_{unlike}$ for each event. An unbinned maximum-likelihood fit is then performed to extract the oscillation frequency Δm_d .

Results and Systematic Errors for Δm_d

In Figure 4 the distribution of decay times for all leptons in the dilepton sample is plotted for like-sign $(N^{++} + N^{--})$ and unlike-sign $(N^{+-} + N^{-+})$ events, where N^{++}, N^{--}, N^{+-} and N^{-+} are numbers of dilepton events with different leptons charge combinations. There are 483 reconstructed vertices in the like-sign events and 946 in the unlike-sign events. Events when both decay times have been reconstructed for both leptons enter the plots twice. The fit results are shown by the superimposed curves. The ratio of like-sign dileptons to the total number of dilepton events as a function of the proper time is shown in Figure 5. The expected variation with proper time is clearly observed. Individual contributions to the distribution from different sources (see Table 3) are shown on the same plot.

In the fit to the data the value for the oscillation frequency of $\mathrm{B_s^0}$ mesons was fixed to 10 ps^{-1}, thus assuming a large mixing in the $\mathrm{B_s^0}$ system. The B lifetime was fixed to the $\mathrm{B^0}$ world average value $\tau_{B^0} = 1.58 \pm 0.05$ ps [13].

To find Δm_d a four-parameter fit was performed. The fitted parameters are Δm_d, the $\mathrm{B_d^0}$ and $\mathrm{B_s^0}$ fractions in $\mathrm{b\bar{b}}$ events f_d and f_s and the cascade fraction F_{bcl}. The oscillation frequency Δm_d is a free parameter; for the other three parameters Gaussian constraints are applied. The fractions f_d and f_s are set to the ones derived from $\mathrm{D_s}$-lepton and Λ_c-lepton correlations measured by the ALEPH [14] experiment. The result of the fit is given in Table 4. The error

Parameter	Fit result	Constraint
Δm_d	$0.496^{+0.066}_{-0.063}$ ps^{-1}	free
f_d	0.391 ± 0.024	0.388 ± 0.025
f_s	0.122 ± 0.024	0.11 ± 0.028
F_{bcl}	$F_{bcl}^{MC} * (0.97 \pm 0.14)$	$F_{bcl}^{MC} * (1. \pm 0.15)$

Table 4: The result of the fit for the data. F_{bcl}^{MC} is the relative fraction of cascade decays as derived from Monte Carlo.

on Δm_d includes the statistical error as well as a contribution from the errors of the fitted fractions. To separate out the statistical error we fix all fractions to their fitted values and repeat the fit. This gives

$$\Delta m_d = 0.496^{+0.055}_{-0.051}\ (\mathrm{stat})\ \mathrm{ps}^{-1}$$

where the error is purely statistical. The systematic error on Δm_d resulting from the fitted fractions is then obtained by subtracting in quadrature the statistical error. Its value is 0.037. This method accounts for the strong correlation between these three sources of systematic error. Individual contributions due to variations of each fraction are $\pm 0.017, \pm 0.037$ and ± 0.018 for f_d, f_s and F_{bcl} respectively.

The other contributions to the systematic error on Δm_d, given in Table 5, are obtained as follows. The variation of the fractions was taken to be $\pm 30\%$ for fake leptons and $\mathrm{c\bar{c}}$ events and $\pm 50\%$ for light-quarks events. Contributions to the systematic error from the time resolution were estimated by changing the widths of the resolution function by $\pm 25\%$. The B momentum

Source of uncertainty	Variation of Δm_d [ps^{-1}]	
B_d^0 fraction (f_d) B_s^0 fraction (f_s) cascade decay fraction (F_{bcl})	-0.036	$+0.037$
fakes fraction	-0.009	$+0.007$
$c\bar{c}$ fraction	$+0.001$	-0.001
uds fraction	-0.001	$+0.001$
B life time	-0.004	$+0.004$
time resolution	$+0.008$	-0.007
B momentum	$+0.015$	-0.014
w_{bl}	-0.002	$+0.002$
w_{bcl}	-0.010	$+0.009$
w_{bfk}	-0.010	$+0.009$
w_{udsc}	-0.001	$+0.001$
Δm_s	-0.001	$+0.001$
total	$+0.043$	-0.043

Table 5: Summary of contributions to the systematic error on Δm_d. The left column corresponds to an increased and right one to a decreased value of the parameter under study. The total errors are calculated as the quadratic sum of all positive and negative contributions, respectively.

contribution was estimated by changing the average fraction of the beam energy carried by the b-hadrons by ± 0.03. The charge confusion factor w_{bl} was varied within $\pm 30\%$. The other w factors were changed by an estimate of their relative uncertainty: ± 0.05 for w_{bcl}, ± 0.10 for w_{bfk}, and ± 0.10 for w_{udsc}. The variation of Δm_s from 3 to 20 ps^{-1} gives a negligible contribution to the systematic error.

The final result of the Δm_d measurement including the systematic error is

$$\Delta m_d = \left(0.496^{+0.055}_{-0.051}\ (\mathrm{stat}) \pm 0.043\ (\mathrm{syst})\right)\ \mathrm{ps}^{-1}$$

The data exclude the hypothesis of no time dependence of mixing at the 99.9% confidence level as calculated from the difference in the values of the likelihood in a fit with and without time dependent mixing. The result for Δm_d is in good agreement with the results of other experiments [15].

Several consistency checks were made. A fit on a Monte Carlo sample of 2.5 million hadronic events gives $\Delta m_d = 0.442 \pm 0.041$ ps^{-1} and reproduces well the input value of $\Delta m_d = 0.452$ ps^{-1}.

As a cross check on a potential bias of the method, the lifetime was also determined from the data and from the Monte Carlo sample of inclusive lepton events. For the Monte Carlo sample the fit gives $\tau_B = 1.552 \pm 0.013$ ps for a Monte Carlo input of 1.55 ps for all b-hadrons.

For the data a one-parameter fit gives 1.584 ± 0.018 ps where the error is statistical only and is consistent with our previously published result [16].

To check the stability of the result with respect to the cut on the lepton transverse momentum, the four-parameter fit was repeated with different values of the cut. The results are given in Table 6. The measurement of Δm_d is stable within errors with respect to this cut.

p_t cut [GeV]	$\Delta m_d[\mathrm{ps}^{-1}]$
0.75	0.483 ± 0.069
1.00	0.496 ± 0.064
1.25	0.495 ± 0.062
1.50	0.480 ± 0.072

Table 6: Stability with respect to the p_t cut. A four-parameter fit is performed (see text).

Conclusion

The time-dependent $\mathrm{B_d^0}$-$\mathrm{\bar{B}_d^0}$ mixing has been studied from the decay lengths reconstructed using the silicon microvertex detector with same-sign and opposite-sign dilepton events. The oscillation frequency is measured to be

$$\Delta m_d = \left(0.496^{+0.055}_{-0.051}\ (\mathrm{stat}) \pm 0.043\ (\mathrm{syst})\right)\ \mathrm{ps}^{-1}\ .$$

Acknowledgements

We wish to express our gratitude to the CERN accelerator divisions for the excellent performance of the LEP machine. We also acknowledge and appreciate the effort of the all engineers, technicians and support staff who have participated in the construction and maintenance of this experiment. Those of us who are not from member states thank CERN for its hospitality and help.

References

[1] UA1 Collaboration, C. Albajar *et al.*, Phys. Lett. **B 186** (1987) 247.

[2] ARGUS Collaboration, H. Albrecht *et al.*, Phys. Lett. **B 192** (1987) 245;
ARGUS Collaboration, H. Albrecht *et al.*, Phys. Lett. **B 324** (1994) 249;
CLEO Collaboration, J. Bartelt *et al.*, Phys. Rev. **D 50** (1994) 43.

[3] ALEPH Collaboration, D. Decamp *et al.*, Phys. Lett. **B 284** (1992) 177;
DELPHI Collaboration, P. Abreu *et al.*, Phys. Lett. **B 332** (1994) 488;
L3 Collaboration, M. Acciarri *et al.*, Phys. Lett. **B 335** (1994) 542;
OPAL Collaboration, R. Akers *et al.*, Z. Phys. **C 60** (1993) 199.

[4] ALEPH Collaboration, D. Buskulic *et al.*, Phys. Lett. **B 313** (1993) 498;
ALEPH Collaboration, D. Buskulic *et al.*, Phys. Lett. **B 322** (1994) 441.

[5] DELPHI Collaboration, P. Abreu *et al.*, Phys. Lett. **B 338** (1994) 409.

[6] OPAL Collaboration, R. Akers *et al.*, Phys. Lett. **B 327** (1994) 411;
OPAL Collaboration, R. Akers *et al.*, Phys. Lett. **B 336** (1994) 585;
OPAL Collaboration, R. Akers *et al.*, Z. Phys. **C 66** (1995) 555.

[7] L3 Collaboration, B. Adeva *et al.*, Nucl. Instr. and Meth. **A 289** (1990) 35;
L3 Collaboration, O. Adriani *et al.*, Phys. Rep. **236** (1993) 1.

[8] M. Acciarri *et al.*, Nucl. Instr. and Meth. **A 351** (1994) 300.

[9] T. Sjöstrand, Comput. Phys. Commun. **39** (1986) 347;
T. Sjöstrand and M. Bengtsson, Comput. Phys. Commun. **43** (1987) 367.

[10] The L3 detector simulation is based on GEANT Version 3.14; see R. Brun *et al.*, GEANT 3, CERN DD/EE/84-1 (Revised), September 1987 and the GHEISHA program (H. Fesefeld, RWTH Aachen Report PITHA85/02 (1985)) for the simulation of hadronic interactions.

[11] C. Peterson *et al.*, Phys. Rev. **D 27** (1983) 105.

[12] L3 Collaboration, M. Acciarri *et al.*, Phys. Lett. **B 351** (1995) 375.

[13] S. Komamiya, plenary talk at the International Europhysics Conference on High Energy Physics, Brussels, Belgium, 1995, to be published in the proceedings.

[14] ALEPH Collaboration, D. Buskulic *et al.*, Phys. Lett. **B 352** (1995) 479;
ALEPH Collaboration, D. Buskulic *et al.*, Phys. Lett. **B 359** (1995) 236;
ALEPH Collaboration, D. Buskulic *et al.*, Phys. Lett. **B 361** (1995) 221.

[15] R. Aleksan, plenary talk at the International Europhysics Conference on High Energy Physics, Brussels, Belgium, 1995, to be published in the proceedings.

[16] L3 Collaboration, O. Adriani *et al.*, Phys. Lett. **B 317** (1993) 474.

The L3 Collaboration:

M.Acciarri,[28] O.Adriani,[17] M.Aguilar-Benitez,[27] S.Ahlen,[11] B.Alpat,[35] J.Alcaraz,[27] G.Alemanni,[23] J.Allaby,[18]
A.Aloisio,[30] G.Alverson,[12] M.G.Alviggi,[30] G.Ambrosi,[20] H.Anderhub,[50] V.P.Andreev,[47,39] T.Angelescu,[13]
D.Antreasyan,[9] A.Arefiev,[29] T.Azemoon,[3] T.Aziz,[10] P.Bagnaia,[38] L.Baksay,[45] R.C.Ball,[3] S.Banerjee,[10] K.Banicz,[47]
R.Barillère,[18] L.Barone,[38] P.Bartalini,[35] A.Baschirotto,[28] M.Basile,[9] R.Battiston,[35] A.Bay,[23] F.Becattini,[17] U.Becker,[16]
F.Behner,[50] J.Berdugo,[27] P.Berges,[16] B.Bertucci,[18] B.L.Betev,[50] M.Biasini,[18] A.Biland,[50] G.M.Bilei,[35] J.J.Blaising,[18]
S.C.Blyth,[36] G.J.Bobbink,[2] R.Bock,[1] A.Böhm,[1] B.Borgia,[38] A.Boucham,[4] D.Bourilkov,[50] M.Bourquin,[20] D.Boutigny,[4]
E.Brambilla,[16] J.G.Branson,[41] V.Brigljevic,[50] I.C.Brock,[36] A.Buijs,[46] J.D.Burger,[16] W.J.Burger,[20] J.Busenitz,[45]
A.Buytenhuijs,[32] X.D.Cai,[19] M.Campanelli,[50] M.Capell,[16] G.Cara Romeo,[9] M.Caria,[35] G.Carlino,[4] A.M.Cartacci,[17]
J.Casaus,[27] G.Castellini,[17] R.Castello,[28] F.Cavallari,[38] N.Cavallo,[30] C.Cecchi,[20] M.Cerrada,[27] F.Cesaroni,[24]
M.Chamizo,[27] A.Chan,[52] Y.H.Chang,[52] U.K.Chaturvedi,[19] M.Chemarin,[26] A.Chen,[52] G.Chen,[7] G.M.Chen,[7]
H.F.Chen,[21] H.S.Chen,[7] M.Chen,[16] G.Chiefari,[30] C.Y.Chien,[5] M.T.Choi,[44] L.Cifarelli,[40] F.Cindolo,[9] C.Civinini,[17]
I.Clare,[16] R.Clare,[16] H.O.Cohn,[33] G.Coignet,[4] A.P.Colijn,[2] N.Colino,[27] S.Costantini,[38] F.Cotorobai,[13] B.de la Cruz,[27]
A.Csilling,[14] T.S.Dai,[16] R.D'Alessandro,[17] R.de Asmundis,[30] H.De Boeck,[32] A.Degré,[4] K.Deiters,[48] P.Denes,[37]
F.DeNotaristefani,[38] D.DiBitonto,[45] M.Diemoz,[38] D.van Dierendonck,[2] F.Di Lodovico,[50] C.Dionisi,[38] M.Dittmar,[50]
A.Dominguez,[41] A.Doria,[30] I.Dorne,[4] M.T.Dova,[19,♯] E.Drago,[30] D.Duchesneau,[4] P.Duinker,[2] I.Duran,[42] S.Dutta,[10]
S.Easo,[35] Yu.Efremenko,[33] H.El Mamouni,[26] A.Engler,[36] F.J.Eppling,[16] F.C.Erné,[2] J.P.Ernenwein,[26] P.Extermann,[20]
M.Fabre,[48] R.Faccini,[38] S.Falciano,[38] A.Favara,[17] J.Fay,[26] O.Fedin,[39] M.Felcini,[50] T.Ferguson,[36] D.Fernandez,[27]
F.Ferroni,[38] H.Fesefeldt,[1] E.Fiandrini,[35] J.H.Field,[20] F.Filthaut,[36] P.H.Fisher,[16] G.Forconi,[16] L.Fredj,[20]
K.Freudenreich,[50] C.Furetta,[28] Yu.Galaktionov,[29,16] S.N.Ganguli,[10] S.S.Gau,[12] S.Gentile,[38] J.Gerald,[5]
N.Gheordanescu,[13] S.Giagu,[38] S.Goldfarb,[23] J.Goldstein,[11] Z.F.Gong,[21] A.Gougas,[5] G.Gratta,[34] M.W.Gruenewald,[8]
V.K.Gupta,[37] A.Gurtu,[10] L.J.Gutay,[47] K.Hangarter,[1] B.Hartmann,[1] A.Hasan,[31] T.Hebbeker,[8] A.Hervé,[18]
W.C.van Hoek,[32] H.Hofer,[50] H.Hoorani,[20] S.R.Hou,[52] G.Hu,[19] M.M.Ilyas,[19] V.Innocente,[18] H.Janssen,[4] B.N.Jin,[7]
L.W.Jones,[3] P.de Jong,[16] I.Josa-Mutuberria,[27] A.Kasser,[23] R.A.Khan,[19] Yu.Kamyshkov,[33] P.Kapinos,[49]
J.S.Kapustinsky,[25] Y.Karyotakis,[4] M.Kaur,[19,◇] M.N.Kienzle-Focacci,[20] D.Kim,[5] J.K.Kim,[44] S.C.Kim,[44] Y.G.Kim,[44]
W.W.Kinnison,[25] A.Kirkby,[34] D.Kirkby,[34] J.Kirkby,[18] D.Kiss,[14] W.Kittel,[32] A.Klimentov,[16,29] A.C.König,[32]
I.Korolko,[29] V.Koutsenko,[16,29] R.W.Kraemer,[36] T.Kramer,[16] W.Krenz,[1] H.Kuijten,[32] A.Kunin,[16,29]
P.Ladron de Guevara,[27] G.Landi,[17] C.Lapoint,[16] K.Lassila-Perini,[50] P.Laurikainen,[22] M.Lebeau,[18] A.Lebedev,[16]
P.Lebrun,[26] P.Lecomte,[50] P.Lecoq,[18] P.Le Coultre,[50] J.S.Lee,[44] K.Y.Lee,[44] C.Leggett,[3] J.M.Le Goff,[18] R.Leiste,[49]
M.Lenti,[17] E.Leonardi,[38] P.Levtchenko,[39] C.Li,[21] E.Lieb,[49] W.T.Lin,[52] F.L.Linde,[2,18] L.Lista,[30] Z.A.Liu,[7]
W.Lohmann,[49] E.Longo,[38] W.Lu,[34] Y.S.Lu,[7] K.Lübelsmeyer,[1] C.Luci,[38] D.Luckey,[16] L.Ludovici,[38] L.Luminari,[38]
W.Lustermann,[48] W.G.Ma,[21] A.Macchiolo,[17] M.Maity,[10] G.Majumder,[10] L.Malgeri,[38] A.Malinin,[29] C.Maña,[27]
S.Mangla,[10] P.Marchesini,[50] A.Marin,[11] J.P.Martin,[26] F.Marzano,[38] G.G.G.Massaro,[2] K.Mazumdar,[10] D.McNally,[18]
S.Mele,[30] L.Merola,[30] M.Meschini,[17] W.J.Metzger,[32] M.von der Mey,[1] Y.Mi,[23] A.Mihul,[13] A.J.W.van Mil,[32]
G.Mirabelli,[38] J.Mnich,[18] B.Monteleoni,[17] R.Moore,[3] S.Morganti,[38] R.Mount,[34] S.Müller,[1] F.Muheim,[20] E.Nagy,[14]
S.Nahn,[16] M.Napolitano,[30] F.Nessi-Tedaldi,[50] H.Newman,[34] A.Nippe,[1] H.Nowak,[49] G.Organtini,[38] R.Ostonen,[22]
D.Pandoulas,[1] S.Paoletti,[38] P.Paolucci,[30] H.K.Park,[36] G.Pascale,[38] G.Passaleva,[17] S.Patricelli,[30] T.Paul,[12]
M.Pauluzzi,[35] C.Paus,[1] F.Pauss,[50] D.Peach,[18] Y.J.Pei,[1] S.Pensotti,[28] D.Perret-Gallix,[4] S.Petrak,[8] A.Pevsner,[5]
D.Piccolo,[30] M.Pieri,[17] J.C.Pinto,[36] P.A.Piroué,[37] E.Pistolesi,[17] V.Plyaskin,[29] M.Pohl,[50] V.Pojidaev,[29,17] H.Postema,[16]
N.Produit,[20] D.Prokofiev,[39] R.Raghavan,[10] G.Rahal-Callot,[50] P.G.Rancoita,[28] M.Rattaggi,[28] G.Raven,[41]
P.Razis,[31] K.Read,[33] D.Ren,[50] M.Rescigno,[38] S.Reucroft,[12] T.van Rhee,[46] S.Riemann,[49] B.C.Riemers,[47] K.Riles,[3]
O.Rind,[3] S.Ro,[44] A.Robohm,[50] J.Rodin,[16] F.J.Rodriguez,[27] B.P.Roe,[3] S.Röhner,[1] L.Romero,[27] S.Rosier-Lees,[4]
Ph.Rosselet,[23] W.van Rossum,[46] S.Roth,[1] J.A.Rubio,[18] H.Rykaczewski,[50] J.Salicio,[18] E.Sanchez,[27] A.Santocchia,[35]
M.E.Sarakinos,[22] S.Sarkar,[10] M.Sassowsky,[1] G.Sauvage,[4] C.Schäfer,[1] V.Schegelsky,[39] S.Schmidt-Kaerst,[1] D.Schmitz,[1]
P.Schmitz,[1] M.Schneegans,[4] B.Schoeneich,[49] N.Scholz,[50] H.Schopper,[51] D.J.Schotanus,[32] J.Schwenke,[1] G.Schwering,[1]
C.Sciacca,[30] D.Sciarrino,[20] J.C.Sens,[52] L.Servoli,[35] S.Shevchenko,[34] N.Shivarov,[43] V.Shoutko,[29] J.Shukla,[25]
E.Shumilov,[29] A.Shvorob,[34] T.Siedenburg,[1] D.Son,[44] A.Sopczak,[49] V.Soulimov,[30] B.Smith,[16] P.Spillantini,[17]
M.Steuer,[16] D.P.Stickland,[37] F.Sticozzi,[16] H.Stone,[37] B.Stoyanov,[43] A.Straessner,[1] K.Strauch,[15] K.Sudhakar,[10]
G.Sultanov,[19] L.Z.Sun,[21] G.F.Susinno,[20] H.Suter,[50] J.D.Swain,[19] X.W.Tang,[7] L.Tauscher,[6] L.Taylor,[12]
Samuel C.C.Ting,[16] S.M.Ting,[16] F.Tonisch,[49] M.Tonutti,[1] S.C.Tonwar,[10] J.Tóth,[14] C.Tully,[37] H.Tuchscherer,[45]
K.L.Tung,[7] J.Ulbricht,[50] U.Uwer,[18] E.Valente,[38] R.T.Van de Walle,[32] G.Vesztergombi,[14] I.Vetlitsky,[29] G.Viertel,[50]
M.Vivargent,[4] R.Völkert,[49] H.Vogel,[36] H.Vogt,[49] I.Vorobiev,[29] A.A.Vorobyov,[39] A.Vorvolakos,[31] M.Wadhwa,[6]
W.Wallraff,[1] J.C.Wang,[16] X.L.Wang,[21] Y.F.Wang,[16] Z.M.Wang,[21] A.Weber,[1] F.Wittgenstein,[18] S.X.Wu,[19]
S.Wynhoff,[1] J.Xu,[11] Z.Z.Xu,[21] B.Z.Yang,[21] C.G.Yang,[7] X.Y.Yao,[7] J.B.Ye,[21] S.C.Yeh,[52] J.M.You,[36] An.Zalite,[39]
Yu.Zalite,[39] P.Zemp,[50] Y.Zeng,[1] Z.Zhang,[7] Z.P.Zhang,[21] B.Zhou,[11] Y.Zhou,[3] G.Y.Zhu,[7] R.Y.Zhu,[34] A.Zichichi.[9,18,19]

1 I. Physikalisches Institut, RWTH, D-52056 Aachen, FRG[§]
III. Physikalisches Institut, RWTH, D-52056 Aachen, FRG[§]
2 National Institute for High Energy Physics, NIKHEF, and University of Amsterdam, NL-1009 DB Amsterdam, The Netherlands
3 University of Michigan, Ann Arbor, MI 48109, USA
4 Laboratoire d'Annecy-le-Vieux de Physique des Particules, LAPP,IN2P3-CNRS, BP 110, F-74941 Annecy-le-Vieux CEDEX, France
5 Johns Hopkins University, Baltimore, MD 21218, USA
6 Institute of Physics, University of Basel, CH-4056 Basel, Switzerland
7 Institute of High Energy Physics, IHEP, 100039 Beijing, China[△]
8 Humboldt University, D-10099 Berlin, FRG[§]
9 INFN-Sezione di Bologna, I-40126 Bologna, Italy
10 Tata Institute of Fundamental Research, Bombay 400 005, India
11 Boston University, Boston, MA 02215, USA
12 Northeastern University, Boston, MA 02115, USA
13 Institute of Atomic Physics and University of Bucharest, R-76900 Bucharest, Romania
14 Central Research Institute for Physics of the Hungarian Academy of Sciences, H-1525 Budapest 114, Hungary[‡]
15 Harvard University, Cambridge, MA 02139, USA
16 Massachusetts Institute of Technology, Cambridge, MA 02139, USA
17 INFN Sezione di Firenze and University of Florence, I-50125 Florence, Italy
18 European Laboratory for Particle Physics, CERN, CH-1211 Geneva 23, Switzerland
19 World Laboratory, FBLJA Project, CH-1211 Geneva 23, Switzerland
20 University of Geneva, CH-1211 Geneva 4, Switzerland
21 Chinese University of Science and Technology, USTC, Hefei, Anhui 230 029, China[△]
22 SEFT, Research Institute for High Energy Physics, P.O. Box 9, SF-00014 Helsinki, Finland
23 University of Lausanne, CH-1015 Lausanne, Switzerland
24 INFN-Sezione di Lecce and Universitá Degli Studi di Lecce, I-73100 Lecce, Italy
25 Los Alamos National Laboratory, Los Alamos, NM 87544, USA
26 Institut de Physique Nucléaire de Lyon, IN2P3-CNRS,Université Claude Bernard, F-69622 Villeurbanne, France
27 Centro de Investigaciones Energeticas, Medioambientales y Tecnologicas, CIEMAT, E-28040 Madrid, Spain[♭]
28 INFN-Sezione di Milano, I-20133 Milan, Italy
29 Institute of Theoretical and Experimental Physics, ITEP, Moscow, Russia
30 INFN-Sezione di Napoli and University of Naples, I-80125 Naples, Italy
31 Department of Natural Sciences, University of Cyprus, Nicosia, Cyprus
32 University of Nymegen and NIKHEF, NL-6525 ED Nymegen, The Netherlands
33 Oak Ridge National Laboratory, Oak Ridge, TN 37831, USA
34 California Institute of Technology, Pasadena, CA 91125, USA
35 INFN-Sezione di Perugia and Universitá Degli Studi di Perugia, I-06100 Perugia, Italy
36 Carnegie Mellon University, Pittsburgh, PA 15213, USA
37 Princeton University, Princeton, NJ 08544, USA
38 INFN-Sezione di Roma and University of Rome, "La Sapienza", I-00185 Rome, Italy
39 Nuclear Physics Institute, St. Petersburg, Russia
40 University and INFN, Salerno, I-84100 Salerno, Italy
41 University of California, San Diego, CA 92093, USA
42 Dept. de Fisica de Particulas Elementales, Univ. de Santiago, E-15706 Santiago de Compostela, Spain
43 Bulgarian Academy of Sciences, Central Laboratory of Mechatronics and Instrumentation, BU-1113 Sofia, Bulgaria
44 Center for High Energy Physics, Korea Advanced Inst. of Sciences and Technology, 305-701 Taejon, Republic of Korea
45 University of Alabama, Tuscaloosa, AL 35486, USA
46 Utrecht University and NIKHEF, NL-3584 CB Utrecht, The Netherlands
47 Purdue University, West Lafayette, IN 47907, USA
48 Paul Scherrer Institut, PSI, CH-5232 Villigen, Switzerland
49 DESY-Institut für Hochenergiephysik, D-15738 Zeuthen, FRG
50 Eidgenössische Technische Hochschule, ETH Zürich, CH-8093 Zürich, Switzerland
51 University of Hamburg, D-22761 Hamburg, FRG
52 High Energy Physics Group, Taiwan, China
§ Supported by the German Bundesministerium für Bildung, Wissenschaft, Forschung und Technologie
‡ Supported by the Hungarian OTKA fund under contract number T14459.
♭ Supported also by the Comisión Interministerial de Ciencia y Technologýa
♯ Also supported by CONICET and Universidad Nacional de La Plata, CC 67, 1900 La Plata, Argentina
◇ Also supported by Panjab University, Chandigarh-160014, India
△ Supported by the National Natural Science Foundation of China.

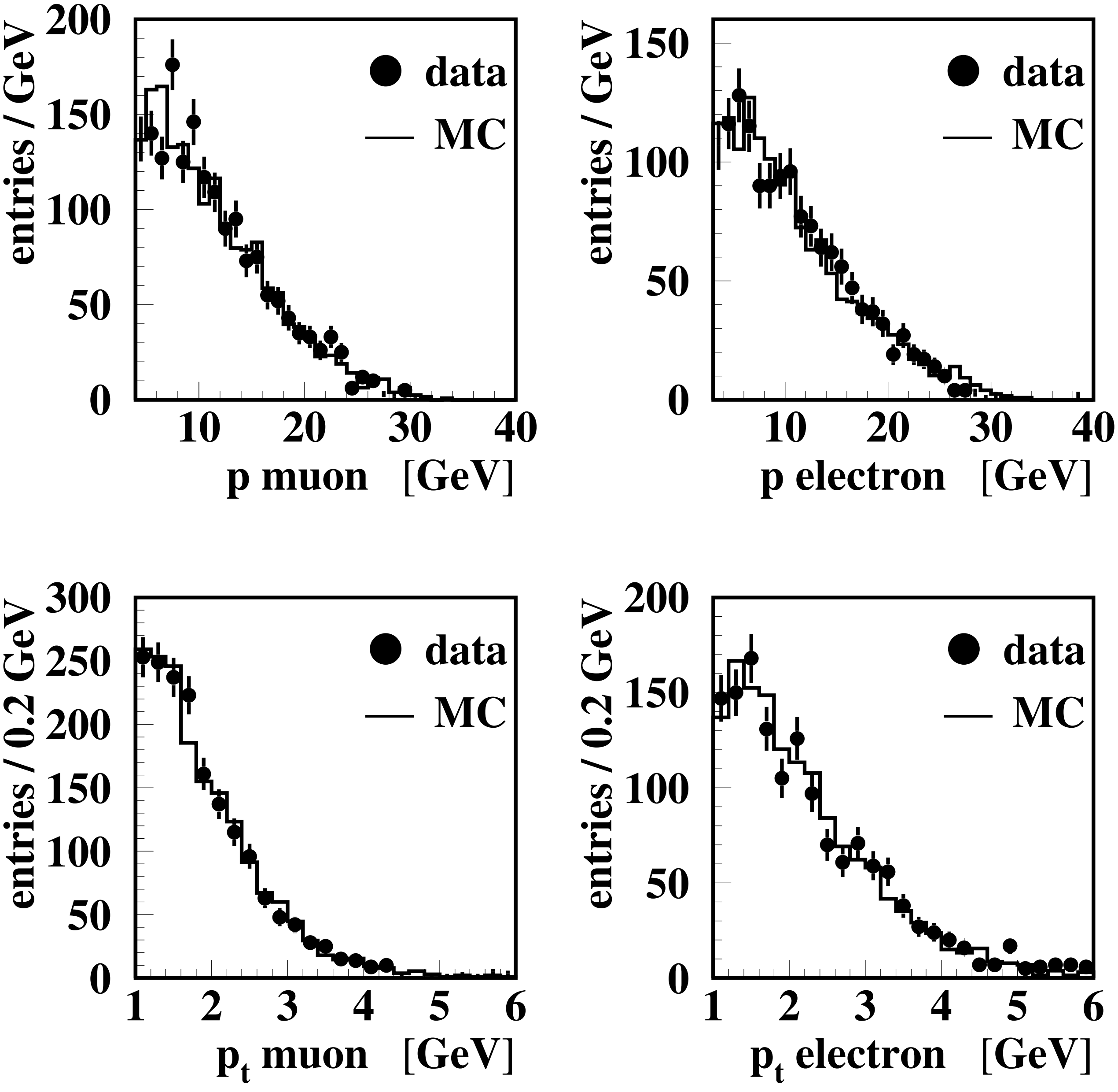

Figure 1: Momentum and transverse momentum spectra of muons and electrons in the selected dilepton events. The Monte Carlo spectra (histograms) are normalized to the same luminosity as the data. The spectra correspond to almost pure $b\bar{b}$ -events (see Table 1). One entry per selected lepton is shown.

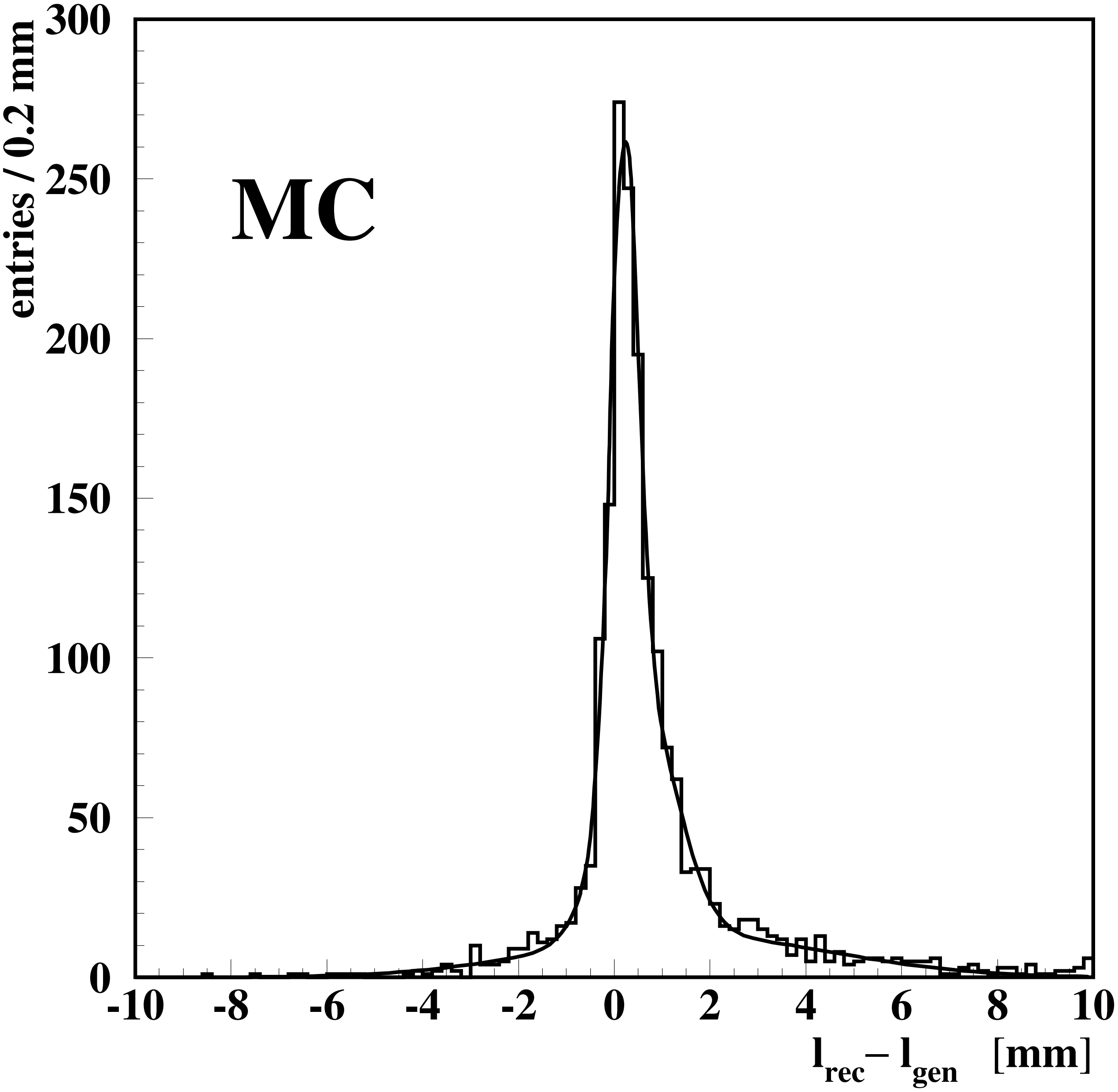

Figure 2: Average decay length resolution for $b\bar{b}$ events in the dilepton sample. The solid line is the result of the fit to the sum of three Gaussians. The fit gives 290 μm, 730 μm and 3.0 mm for the widths, mean values are 0.21 mm, 0.58 mm and 1.56 mm, and the corresponding fractions are 0.38, 0.36 and 0.26 respectively.

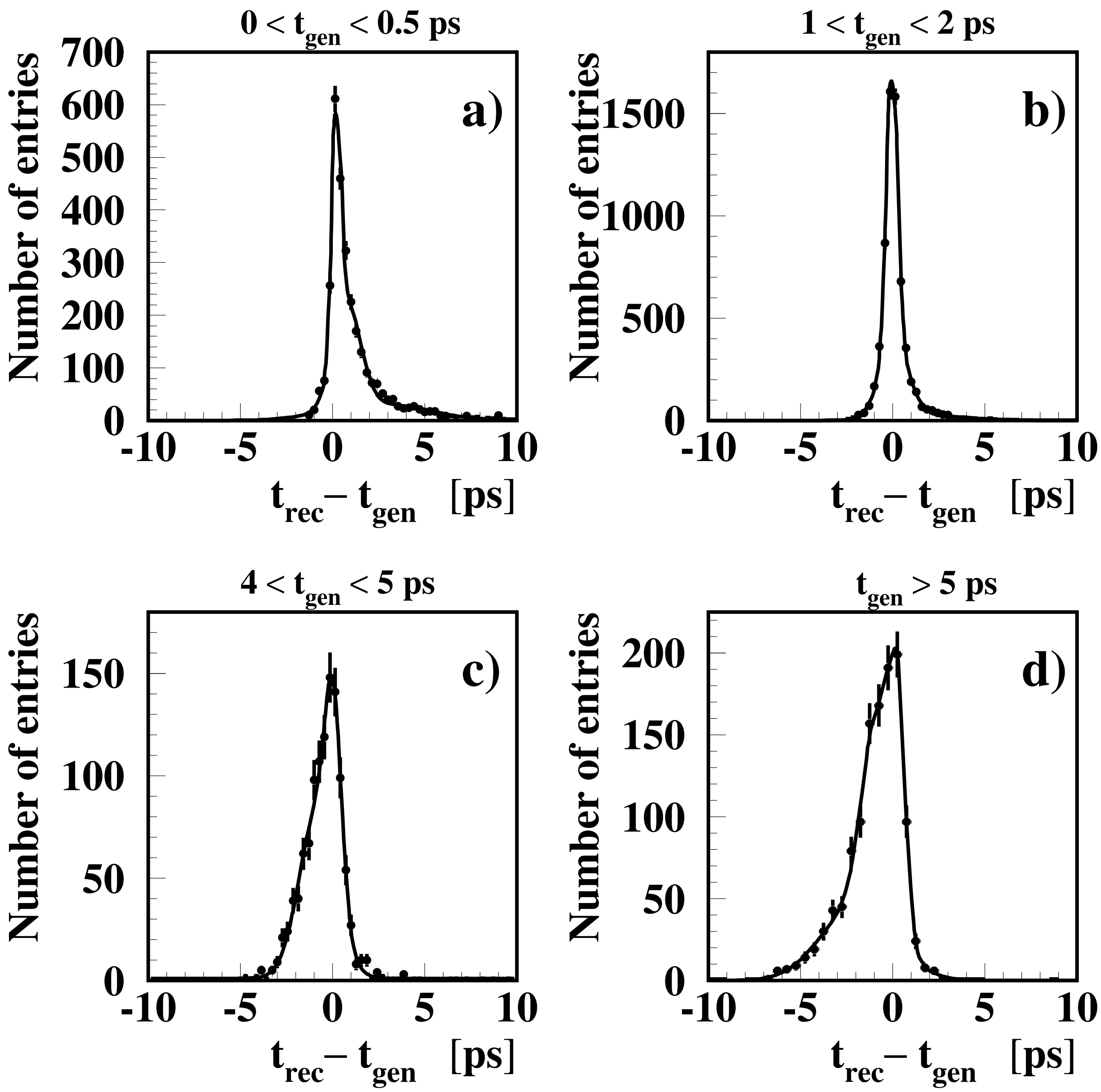

Figure 3: The reconstructed proper time compared to the generated proper time of B decay in four slices of the generated proper time t_{gen} (a) $0 < t_{gen} < 0.5$ ps , b) $1.0 < t_{gen} < 2.0$ ps , c) $4.0 < t_{gen} < 5.0$ ps , d) $t_{gen} > 5.0$ ps). The solid line is the parametrization to a sum of three Gaussians.

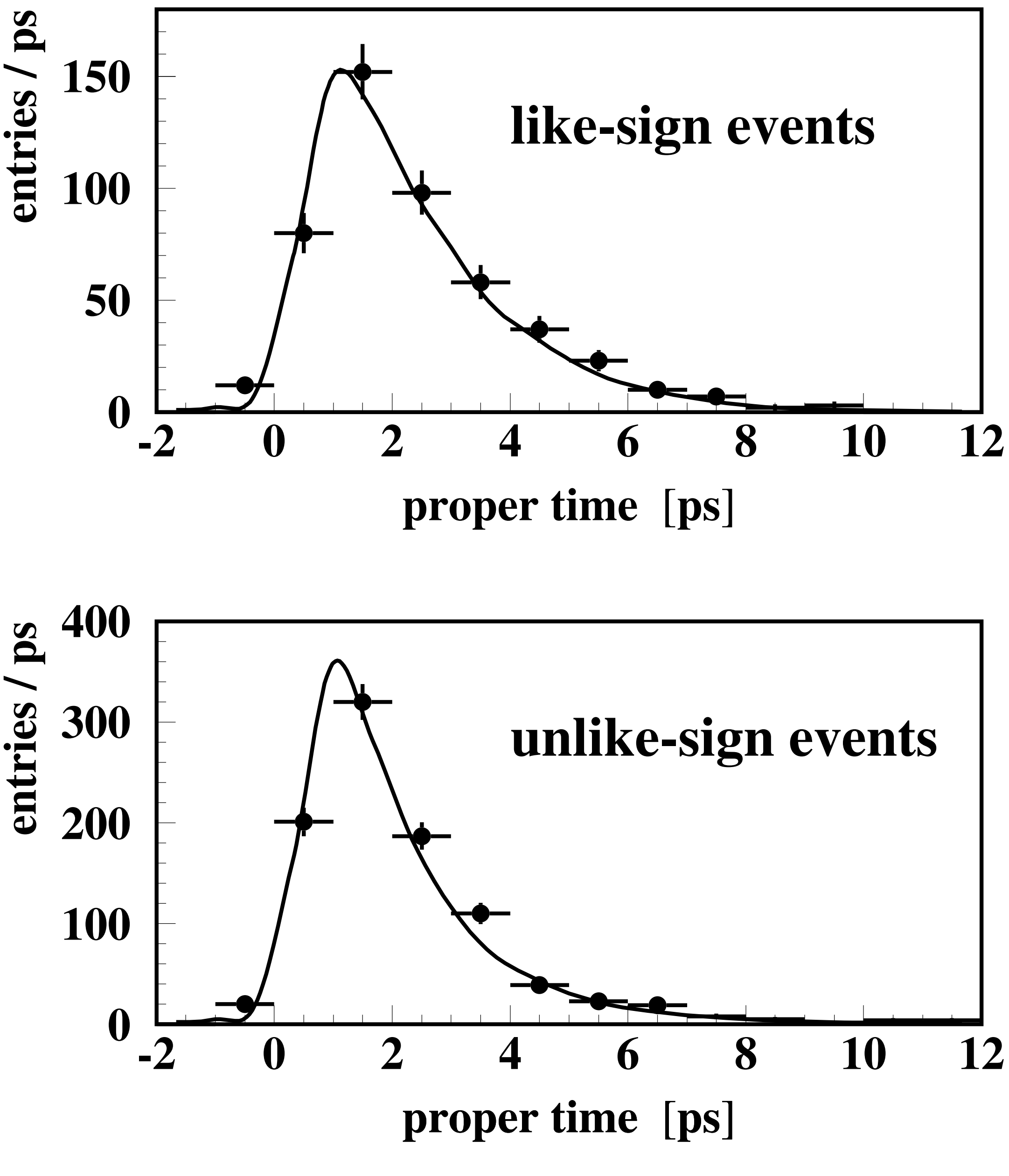

Figure 4: Proper time spectra for like-sign and unlike-sign dilepton events compared to the fit result. Events in which decay times have been reconstructed for both leptons enter the plots twice.

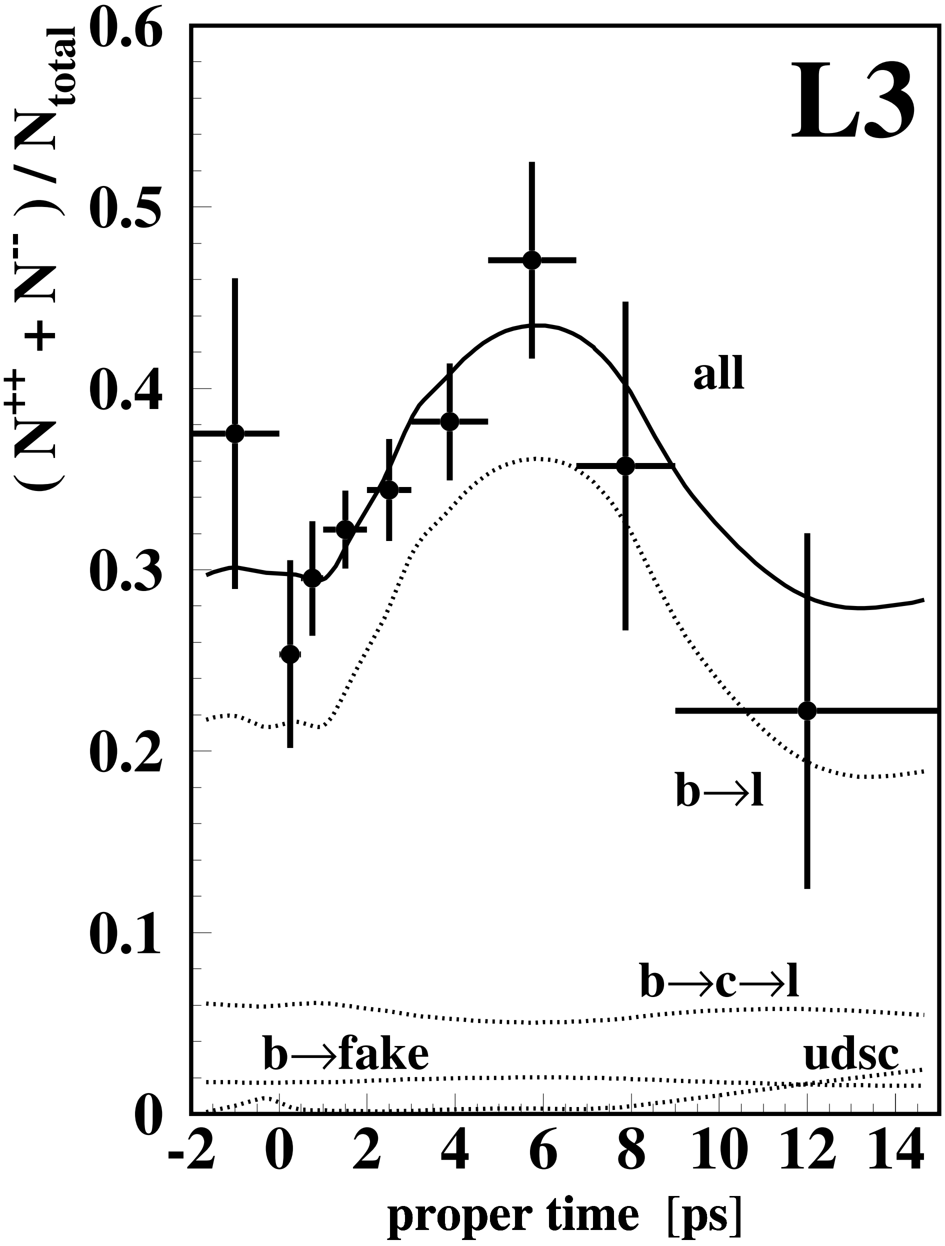

Figure 5: Ratio of same-sign dilepton events to the total number of dilepton events versus the measured proper time compared to the fit result. The solid line is the sum of individual contributions of different sources of such events (see Table 3).